A Current-Based Submodule Selection Algorithm for a Modular Multilevel Converter with Integrated Batteries

1st Niklas Katzenburg
Elektrotechnisches Institut (ETI)
Karlsruhe Institute of Technology (KIT)
Karlsruhe, Germany
niklas.katzenburg@kit.edu

2nd Lars Leister
Elektrotechnisches Institut (ETI)
Karlsruhe Institute of Technology (KIT)
Karlsruhe, Germany
lars.leister@kit.edu

3rd Lukas Stefanski
Elektrotechnisches Institut (ETI)
Karlsruhe Institute of Technology (KIT)
Karlsruhe, Germany
lukas.stefanski@kit.edu

4th Marc Hiller
Elektrotechnisches Institut (ETI)
Karlsruhe Institute of Technology (KIT)
Karlsruhe, Germany
marc.hiller@kit.edu

2025 IEEE 10th Workshop on the Electronic Grid (eGRID) | 979-8-3315-9364-3/25/$31.00 ©2025 IEEE | DOI: 10.1109/eGRID63452.2025.11255590

***Abstract*—As the demand for grid-tied energy storage systems increases, battery storage systems with a multilevel inverter topology based on modular submodules are gaining more attention due to their efficiency and decreased filter demand. These systems allow to combine different types of batteries including second-life batteries, which are likely to have different current limits. This work proposes a new submodule selection algorithm to enforce these limits within a modular multilevel converter with integrated batteries. In contrast to typical algorithms for modular multilevel converters with integrated batteries the presented algorithm considers the battery current and sets it as targeted. This allows to precisely set the operation point of each battery, which is crucial in reducing the aging of the batteries. The proposed, current-based submodule selection algorithm can be combined with any sorting and selection approach for a modular multilevel converter with integrated batteries. Its operating principle is demonstrated by experiments.**

***Index Terms*—Modular Multilevel Converters (MMC), Energy Storage, Modular Reconfigurable Batteries, Submodule Selection Algorithm**

I. Introduction

With the rising demand for grid-tied energy storage systems, modular battery energy storage systems (BESS) have become increasingly popular [1]. One of the respective topologies investigated in research is the modular multilevel converter (MMC) with integrated batteries, henceforth referred to as modular multilevel converter based battery energy storage system (MMC-BESS) [1]–[7]. Integrating batteries into an MMC utilizes the advantages of a traditional MMC, like modularity, easy scalability and high voltage output quality [8], to connect a BESS to the supply grid. At the same time, the degrees of freedom in an MMC-BESS allow individual control of the integrated battery modules, which supports the combination of different battery types as well as the use of second-life batteries [7], [9].

When different types of batteries are combined, the current rating of these batteries might not be the same. The current can either be limited by the specifications of the batteries or by a central energy management system. Especially for second-life batteries or to increase the battery lifetime, it might be sensible to limit the current of some batteries within one arm of an MMC-BESS, where the full arm current would normally flow through all submodules (SMs) contributing to the arm voltage. This current limitation on the SM level is not required in traditional MMCs, because there all SMs are identical and designed to carry the full current. This work proposes an algorithm, which limits the current for individual SMs within an arm of an MMC-BESS, but does not interfere with the sorting of the SMs as desired by the energy management system. Thus, the algorithm presented allows the combination of different types of battery modules within one arm of an MMC-BESS.

Before the proposed algorithm is presented, the topology of an MMC-BESS and existing submodule selection algorithms for MMC-BESS are introduced in section II. Following that introduction, the current limiting algorithm is conceived in section III and simulation as well as experimental results with one arm of an MMC-BESS prototype with an overall energy storage capability of $400\,\mathrm{kWh}$ and a peak power of $100\,\mathrm{kW}$ are presented in section IV.

II. Submodule Selection Algorithms

To perceive the proposed, current-based submodule selection algorithm in section III, it is necessary to understand the fundamentals of MMC-BESS in section II-A and the basic functionality of submodule selection algorithms (SMSAs) in section II-B.

The authors acknowledge the financial support by the Federal Ministry for Economic Affairs and Energy (BMWE) of Germany in the project LeMoStore (03EI4031A-E). The authors are responsible for the content of this publication.

A. The Battery Modular Multilevel Converter

The MMC is a modular converter topology consisting of a large number of identical SMs, which typically consist of a half- or a full-bridge connected to a capacitor [8]. This unit can also be called power electronic module (PEM). As the demand for large scale, gried-tied BESS increases, researchers suggest to extend this converter topology by integrating batteries into the SMs [2], [3]. The batteries can either be connected in parallel to the capacitor of the SM or a DC-DC converter can be used to decouple the battery voltage from the voltage of the SM. SMs with an additional DC-DC converter can also decouple the battery current from the current flowing through the SM, but they cause additional system costs as well as increased losses due to the added semiconductor switches and passive components. This work focuses on MMC-BESS with batteries – or possibly other energy storage modules (ESMs) – directly integrated into the SMs without an additional DC-DC converter as depicted in Fig. 1. This combination of a PEM and an ESM is also called power electronic storage block (PESB). A PESB represents a specific type of SM. In the following sections, the term "SM" denotes the generalization of SMs in traditional MMCs and PESBs in MMC-BESS unless explicitly specified otherwise.

In both types of MMC-BESS and in traditional MMCs the arms are required to generate the voltage desired by the overall control of the system while balancing the capacitors in the SM or batteries in the PESBs. This is achieved by SMSAs, which are explained in the following section.

B. Submodule Selection Algorithms

The SMSA for each arm of the MMC needs to generate the arm voltage requested by the control of the system by selecting appropriate SMs and handling their output voltages. In a traditional MMC the SMSA is also responsible for keeping the capacitor voltages in an acceptable range. Falling below the lower limit will lead to an outage of the SM, exceeding the upper limit will damage the SM. Keeping the capacitor voltage within a safe range is less critical in MMC-BESS, because the battery module integrated into the PESB contains a sufficient amount of energy to stabilize the capacitor voltage.

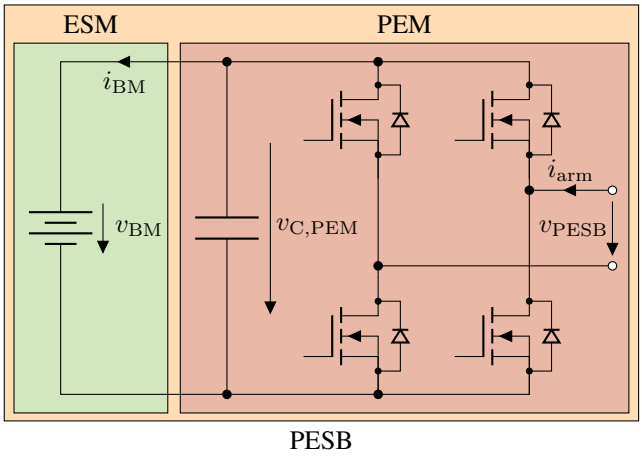

Fig. 1. Power Electronic Storage Block with a battery module as the Energy Storage Module. [7]

In MMC-BESS it is more relevant to select the SMs based on the present and the target condition of the battery. SMSAs typically consider the state of charge (SoC) or the state of health (SoH) of the batteries [6], [9], [10], but combined approaches also exist [11]. Even though a high battery current will result in an increase of the battery temperature, which impacts the aging of the battery, neither the current nor the temperature is explicitly considered in these SMSAs.

In contrast to that, the RMS of the battery current is recognized as a main influence on the heating and thus the aging of the batteries in [12]. To reduce the RMS of the battery currents circulating currents are injected in the MMC-BESS. The sorting and selection of the battery modules is based on an SoC balancing algorithm. However, this approach does not consider specific current limits for different batteries. Individual batteries are taken into account in [13], but are only bypassed when an over-temperature or another fault is registered.

All in all, the aforementioned SMSAs lack the possibility to control the current of each battery module individually. However, this aspect is crucial if different types of batteries or batteries of varying age are combined. In the next section a current-based submodule selection algorithm (CB-SMSA) is proposed to overcome this issue while maintaining the sorting and selection criterion desired by the central energy management system.

III. Proposed Current-Based Submodule Selection Algorithm

As mentioned in section II-A, this work focuses on MMC-BESS with PESBs where the battery is connected in parallel to the capacitor. For this PESB topology, the battery current of the k-th PESB,

$$i_{\mathrm{BM},k} \approx i_{\mathrm{arm}} \cdot d_{\mathrm{PEM},k} = i_{\mathrm{arm}} \cdot \frac{v_{\mathrm{PESB,ref},k}}{v_{\mathrm{C,PEM},k}}\,, \tag{1}$$

depends on the arm current i_{arm} and the PEM's duty cycle $d_{\mathrm{PEM},k}$. The latter can be represented by the quotient of the reference output voltage of the PESB $v_{\mathrm{PESB,ref},k}$ and the capacitor voltage of the PEM $v_{\mathrm{C,PEM},k}$. Therefore, by limiting the PEM's duty cycle and its reference output voltage, respectively, the battery current can be limited for a given arm current. With the battery current limits $i_{\mathrm{BM,lim,d},k} \in \mathbb{R}_0^+$ and $i_{\mathrm{BM,lim,c},k} \in \mathbb{R}_0^+$ for discharging and charging, respectively, the maximum reference output voltage of the k-th PESB,

$$v_{\mathrm{PESB,ref,max},k} = v_{\mathrm{C,PEM},k} \cdot d_{\mathrm{PEM,max},k}\,, \tag{2}$$

can be determined by introducing the auxiliary, maximum duty cycle of the k-th PEM,

$$d_{\mathrm{PEM,max},k} = \begin{cases} \min\left\{\frac{i_{\mathrm{BM,lim,c},k}}{|i_{\mathrm{arm}}|}, 1\right\} & p_{\mathrm{arm,ref}} > 0 \\ 1 & p_{\mathrm{arm,ref}} = 0 \\ \min\left\{\frac{i_{\mathrm{BM,lim,d},k}}{|i_{\mathrm{arm}}|}, 1\right\} & p_{\mathrm{arm,ref}} < 0 \end{cases}. \tag{3}$$

In (3), the reference arm power,

$$p_{\mathrm{arm,ref}} = v_{\mathrm{arm,ref}} \cdot i_{\mathrm{arm}} \,, \tag{4}$$

is introduced to take into account the possibility of a negative arm reference voltage. If it is positive, the battery modules are being charged. It should be noted that the maximum duty cycle and the maximum reference output voltage of the k-th PESB are non-negative values with $d_{\mathrm{PEM,max},k} \in [0,1]$, $v_{\mathrm{PESB,ref,max},k} \in [0, v_{\mathrm{C,PEM},k}] \quad \forall \quad k \in \{1,\ldots,N\}$, where N is the number of PESBs in the arm. The correct sign of the reference output voltage of the k-th PESB is assigned when setting its actual value in (5).

Since the current limitation from (2) and (3) should only be an addition to a regular SMSA for an MMC-BESS, the sorting and the selection of suitable PESBs takes place independently of the current limitation and various criteria, e.g., the SoC and the SoH, can be used to sort the PESBs. However, it is beneficial to employ a more holistic approach optimizing the lifetime of the batteries to determine the sorting order of the PESBs [14]. An approach like that would require the currents of the individual batteries to be precisely set.

For this work, it is assumed that the sorting criterion is determined by a centralized energy management system. This energy management system could also determine the current limits during the operation of the system or fixed current limits can be defined based on the parameters of the battery modules. Here, changing current limits from the centralized energy management system are considered for a more general formulation of the CB-SMSA and for allowing more advanced battery management strategies as introduced in [14].

After determining the maximum reference output voltage $v_{\mathrm{PESB,ref,max},k}$ of each PESB according to (2) and (3) and sorting the PESBs as desired, these pieces of information are merged and the actual reference voltage $v_{\mathrm{PESB,ref}}$ for each PESB is determined in such a way, that the sum of all reference voltages matches the reference arm voltage $v_{\mathrm{arm,ref}}$.

If n PESBs are required to achieve the desired arm reference voltage, i.e., $\sum_{k=1}^{n} v_{\mathrm{PESB,ref,max},k} \geq v_{\mathrm{arm,ref}}$, the reference voltage of the first $n-1$ PESBs is set to

$$v_{\mathrm{PESB,ref},k} = \sigma_{\mathrm{v,arm,ref}} \cdot v_{\mathrm{PESB,ref,max},k} \,, k \in \{1,\ldots,n-1\} \,, \tag{5a}$$

using the auxiliary variable,

$$\sigma_{\mathrm{v,arm,ref}} = \mathrm{sgn}\left(v_{\mathrm{arm,ref}}\right) \,, \tag{5b}$$

to determine the correct sign of the reference output voltage of the corresponding PESB. The reference output voltage of the n-th PESB is set to

$$v_{\mathrm{PESB,ref},n} = v_{\mathrm{arm,ref}} - \sum_{k=1}^{n-1} v_{\mathrm{PESB,ref},k} \,. \tag{5c}$$

In (5c) the sign of the reference output voltage is already correct based on the arm reference voltage and the previously set reference output voltages of the first $n-1$ PESBs. The reference voltage of the possibly remaining PESBs is set to zero. In this way, the desired arm voltage is achieved and the current limits of the batteries are obeyed. However, it should be noted that the switching losses of the arm increase for each PESB where the current limit is enforced. In contrast to regular, unlimited operation, where only one PESB is being switched, i.e., $d_{\mathrm{PEM},k} \in (0,1)$, and the other PESBs are completely turned off or on, i.e., $d_{\mathrm{PEM},k} \in \{0,1\}$, each PESB operating at its current limit is switching.

The battery current limits cannot be infinitely small compared to the maximum arm current,

$$\hat{I}_{\mathrm{arm,max}} = \frac{|i_{\mathrm{dc}}|}{3} + \frac{\hat{I}_{\mathrm{ac}}}{2} \,, \tag{6}$$

which consists of the DC current, i_{dc}, and the grid current with the amplitude $\hat{I}_{\mathrm{ac}}$ in a steady state. To determine lower, worst-case boundaries for the charge and discharge current limits $i_{\mathrm{BM,wcb,c}} \in \mathbb{R}_0^+$ and $i_{\mathrm{BM,wcb,d}} \in \mathbb{R}_0^+$, it must be assumed that all battery modules are operating at their minimum voltage $v_{\mathrm{BM,min}}$. If the DC voltage V_{dc} and the amplitude of the grid voltage $\hat{V}_{\mathrm{ac}}$ of the system are known, the lower, worst-case boundaries for an arm of the MMC-BESS with N PESBs are derived with

$$\sum_{i=1}^{N} \left(\frac{i_{\mathrm{BM,wcb},k}}{\hat{I}_{\mathrm{arm,max}}} \cdot v_{\mathrm{BM,min},k} \right) \geq V_{\mathrm{arm,max}} = 1.05 \cdot \left(\frac{V_{\mathrm{dc}}}{2} + \hat{V}_{\mathrm{ac}} \right) \,, \tag{7}$$

where the auxiliary variable $i_{\mathrm{BM,wcb},k}$ must be replaced by $i_{\mathrm{BM,wcb,d},k}$ for discharging and by $i_{\mathrm{BM,wcb,c},k}$ for charging. The factor 1.05 for the maximum arm voltage $V_{\mathrm{arm,max}}$ is added to allow for some voltage reserve to control the arm current. Condition (7) should be ensured by the design of the system.

During the operation of the arm, (7) can be relaxed to

$$\sum_{i=1}^{N} \left(\frac{i_{\mathrm{BM,lim},k}}{i_{\mathrm{arm}}} \cdot v_{\mathrm{BM},k} \right) \geq v_{\mathrm{arm,ref}} \tag{8}$$

by replacing the minimum voltage of the battery modules with their actual value, the maximum arm voltage $V_{\mathrm{arm,max}}$ with the arm reference voltage and the maximum arm current with the measured arm current i_{arm}. Again, the auxiliary variable $i_{\mathrm{BM,lim},k}$ must be replaced by $i_{\mathrm{BM,lim,d},k}$ for discharging and by $i_{\mathrm{BM,lim,c},k}$ for charging. If the arm reference voltage is used, (8) must be recalculated in every control period T_{ctrl} to ensure the feasibility of the current limits. Vice versa, (8) could be used to determine the control variable saturation for the arm current controller of the overall control of the MMC-BESS. However, the overall control of the MMC-BESS is out of scope and the implementation is not discussed further.

IV. Simulation and Experimental Results

To test the proposed CB-SMSA, an arm with $N = 20$ PESBs of an MMC-BESS with an overall energy storage capability of $400\,\mathrm{kWh}$ and a peak power of $100\,\mathrm{kW}$ [7] is first simulated, then actual measurements with the prototype are presented.

Each PESB consists of a full-bridge and a battery module with a nominal voltage of $v_{\mathrm{BM,nom}} = 51.1\,\mathrm{V}$ and a nominal capacity of $Q_{\mathrm{BM,nom}} = 66\,\mathrm{Ah}$. The actual state of the battery modules at the start of the simulation and their current limits are given in Table I. These values are chosen to match the states and current limits of the actual system during the measurement presented in section IV-B.

TABLE I
PARAMETERS OF THE BATTERY MODULES

PESB	SoC in %	v_{BM} in V	$i_{\mathrm{BM,lim,d}}$ in A	$i_{\mathrm{BM,lim,c}}$ in A
1	52.73	52.48	12	12
2	38.48	50.80	20	20
3	49.55	52.20	3	3
4	45.64	51.64	20	20
5	43.19	51.24	20	20
6	38.97	50.84	10	10
7	39.37	50.87	20	20
8	42.21	51.13	20	20
9	39.08	50.85	20	20
10	40.38	50.94	20	20
11	39.69	51.10	20	20
12	41.77	51.08	20	20
13	38.23	50.88	12	12
14	38.78	50.83	20	20
15	40.85	50.98	20	20
16	38.79	50.83	10	10
17	38.66	50.82	8	8
18	38.83	50.83	20	20
19	39.21	51.05	20	20
20	39.77	50.90	20	20

It can be observed that the PESBs 11, 13 and 19 have a higher voltage than other PESBs with a higher SoC, e.g., PESB 19 has a SoC of $39.21\,\%$ and a voltage of $51.05\,\mathrm{V}$, whereas PESB 7 has a SoC of $39.37\,\%$ and a voltage of $50.87\,\mathrm{V}$.

Since the SoC of the affected modules is within a range of less than $5\,\%$, these discrepancies could be due to the tolerance in estimating the SoC in the real system. Additionally, slight differences in the battery modules' properties, e.g., deviations in the actual capacity compared to the nominal one, could impair the precision of the estimation of the SoC.

A. Simulation

The equivalent circuit used in the simulation is depicted in Fig. 2. It incorporates one arm of the MMC-BESS consisting of 20 PESB and an arm inductance $L_{\mathrm{arm}} = 162\,\mu\mathrm{H}$ and an ideal current source. The arm reference voltage is set to $v_{\mathrm{arm,ref}} = [200 + 150 \cdot \sin(2\pi f t)]\,\mathrm{V}$ with a frequency of $f = 50\,\mathrm{Hz}$. The arm current, $i_{\mathrm{arm}} = [5 + 10 \cdot \sin(2\pi f t)]\,\mathrm{A}$, with the same frequency is fed by the ideal current source.

Both waveforms as well as the output voltages of the PESBs and the respective battery currents are shown in Fig. 3. All quantities except the unfiltered arm voltage v_{arm} are averaged over a control period of $T_{\mathrm{ctrl}} = 125\,\mu\mathrm{s}$.

The order of turning on the PESBs is based on the SoC of these, which is a sorting criterion independent of the proposed CB-SMSA. Battery modules 2, 13, 14 and 17 have the lowest SoC and are turned on at the beginning of the simulation, because with a positive arm voltage and a positive arm current at that time the used battery modules are charged. However, around $0.97\,\mathrm{ms}$ the arm current reaches and exceeds the $8\,\mathrm{A}$ current limit of battery module 17. Thus, the output voltage of PESB 17 is decreased proportionally to the rising arm current to ensure the battery current does not exceed the $8\,\mathrm{A}$ limit.

At the same time, the output voltage of PESB 16 is increased to compensate for the reduced output voltage of PESB 17. Although this effect is difficult to distinguish from the increase in the output voltage due to the rising arm reference voltage, it is still noticeable, because the output voltage step for PESB 16 at this time is higher than the previous one even though the slope of the arm reference voltage is decreasing due to its sinusoidal shape. Next, the output voltage of PESB 18 is starting to increase to follow the arm reference voltage and to compensate the decrease of the output voltage of PESB 17. Starting at $1.76\,\mathrm{ms}$ it also needs to counteract the decrease of the output voltage of PESB 16, which has reached its current limit of $10\,\mathrm{A}$. At around $2\,\mathrm{ms}$, PESB 6 is turned on to follow the arm reference voltage while compensating the reduction of output voltage of the PESBs 17, 16 and 13 due to their respective current limit. However, PESB 6 never reaches its maximum output voltage as its own current limit of $10\,\mathrm{A}$ is hit before that at $2.88\,\mathrm{ms}$ and PESB 9 is used. Lastly, to reach the peak of the arm reference voltage PESB 19 is turned on. As five PESB are turned on with a duty cycle $d_{\mathrm{PEM},k} < 1$ now, many switching events occur, which explains the broad range of the arm voltage around the filtered arm voltage in the first half of the period. Since the arm current does not exceed any current limits anymore after $9.03\,\mathrm{ms}$, the PESBs only reduce their output voltage due to the decreasing arm reference voltage and only one PESB is switching at a time.

For the negative arm current between $11.67\,\mathrm{ms}$ and $18.33\,\mathrm{ms}$ the PESBs with the highest SoC, i.e., PESB 1, 3 and 4, are active, because the arm voltage is still positive and, thus, the battery modules are discharged. However, they are not equally discharged, because the arm reference voltage reaches

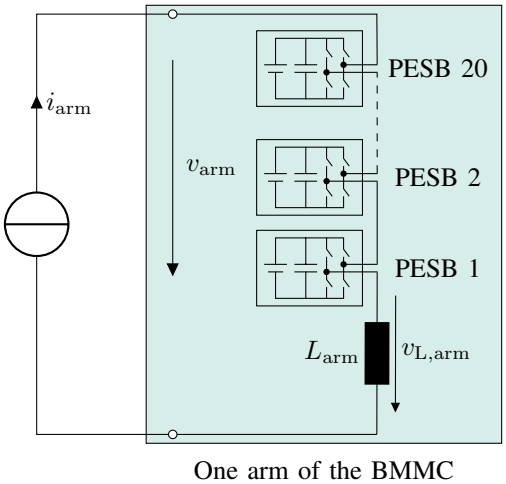

Fig. 2. Equivalent circuit of the simulated system.

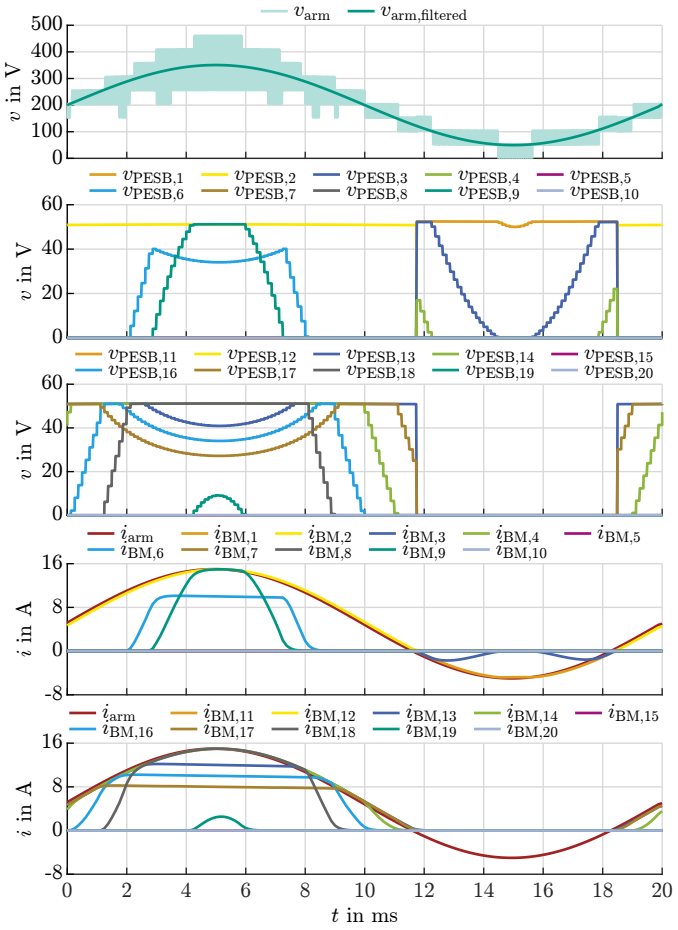

Fig. 3. Simulation results for the proposed, current-based submodule selection algorithm.

its minimum during this duration and the output voltages of the PESBs follow that trajectory. This behavior also reflects in the current of the corresponding battery modules and is particularly evident for PESB 3. It can be seen that the proposed CB-SMSA adheres to the current limits of the battery modules.

B. Experimental Setup and Results

To prove its functionality in a real system, the proposed CB-SMSA is implemented on the FPGA of the Arm Control Unit (ACU) of one arm of an MMC-BESS [7]. The experimental setup is similar to that of the simulation depicted in Fig. 2. Each arm consists of 20 PESBs with battery modules with the same nominal parameters given for the simulation in section IV-A. The cabinet housing the 20 PESBs as well as the ACU is shown in Fig. 4. The initial conditions and the current limits of the battery modules are the same as for the simulation in Table I.

As shown in Fig. 5, the ideal current source is replaced by a two-quadrant emulator of D&V Electronics [15], which can set a unipolar voltage between 0 V and 800 V and a bipolar current with an amplitude of up to ±500 A. The large signal bandwidth is specified with 20 kHz. It operates in voltage

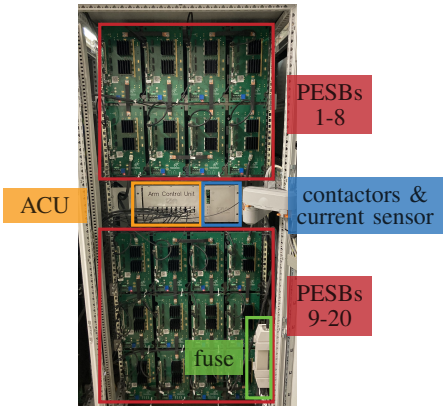

Fig. 4. Electrical cabinet of one arm.

source mode and an additional inductance $L_{\text{emu}} = 1.4\,\text{mH}$ is added in series between the emulator and the arm of the MMC-BESS to improve the current source behavior and to stabilize the control by increasing the time constant of the plant. The respective current control is implemented an OP4510 real-time simulator from OPAL-RT [16], which is coupled with the central control unit (CCU) of the MMC-BESS to allow easy control of the emulator and feed forwarding the arm reference voltage $v_{\text{arm,ref}}$. The latter is generated on the CCU based on user input for this experiment. In the real system, the control of the overall MMC-BESS would be running on the CCU and generating the arm reference voltages for all six arms of the MMC-BESS [7]. In addition to the overall control of the MMC-BESS, the energy management system which estimates the SoC of all battery modules and determines their current limits is also implemented on the CCU. These values are sent to the ACU to be considered in the implemented SMSA.

Fig. 5 includes the main part of the measurement setup, a HBK Gen7tA [17] equipped with five power analyzer cards (GN310B) [19] with three voltage and three current channels each and two voltage cards (GN610B) [20] with six voltage channels each. The power analyzer cards are used to measure the voltages and currents of twelve of the battery modules as well as the arm current and voltage. For the battery currents LA 55-P [21] current transducers are used, for the arm current a DT50ID [22] current transducer. The voltage cards are used to measure the twelve output voltages of the corresponding PESBs. The sample rate of the system is $2\,\text{MSa}\,\text{s}^{-1}$. It is sufficient to measure the quantities of twelve of the PESBs, because the other PESBs are not used in the given scenario anyway. This can be verified by reformulating (8). Based on the information given in Table I and on the simulation results in Fig. 3, it can be determined in advance which PESBs will be active.

The external current source induces an arm current $i_{\text{arm}} = [5 + 10 \cdot \sin(2\pi f t)]\,\text{A}$. The arm reference voltage is set to $v_{\text{arm,ref}} = [200 + 150 \cdot \sin(2\pi f t)]\,\text{V}$. Both have a frequency of $f = 50\,\text{Hz}$. The measured waveforms of the arm voltage, the arm current, the output voltages of the twelve used PESBs currents of the respective battery modules are shown in Fig. 6.

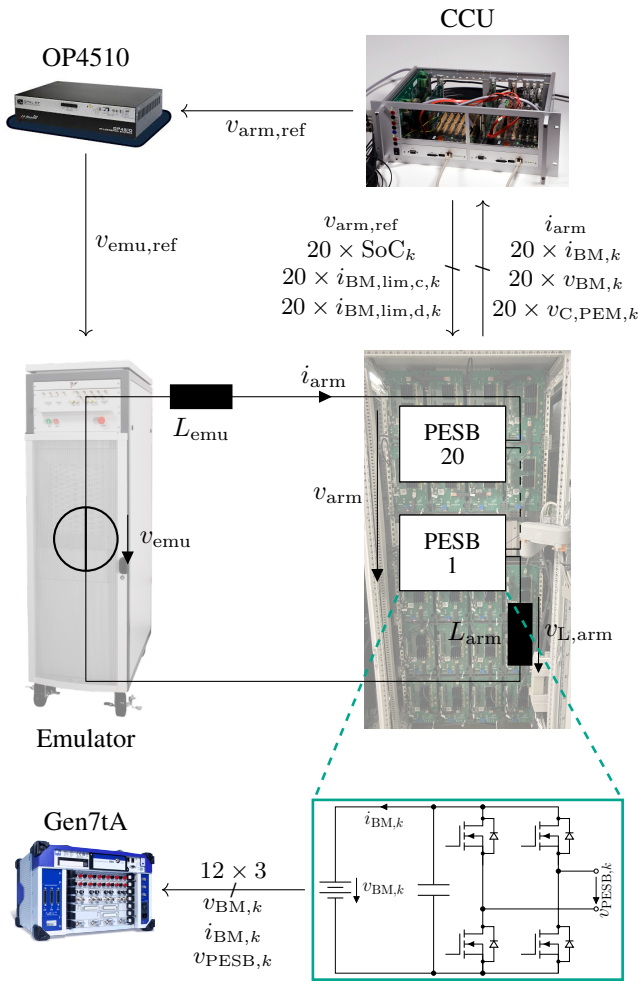

Fig. 5. Experimental setup. [15]–[18]

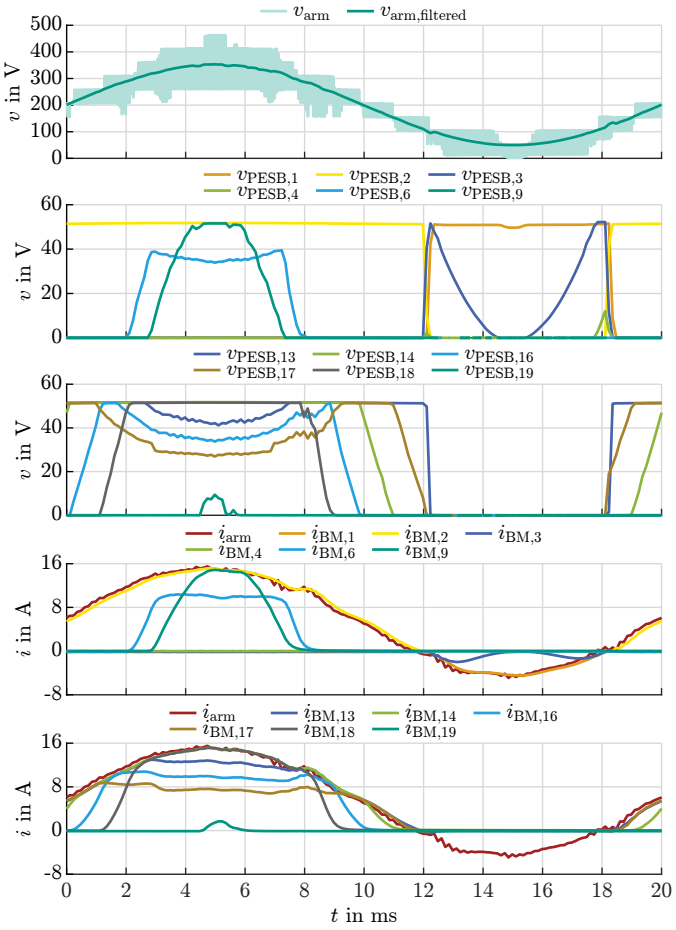

Fig. 6. Exemplary measurement results for the proposed, current-based submodule selection algorithm.

Again, all quantities except the unfiltered arm voltage are averaged over a control period of $T_{\text{ctrl}} = 125\,\mu\text{s}$.

The oscillations in the arm current are due to the interactions between the arm of the MMC-BESS and the emulator. The more significant oscillations in the arm current and the arm voltage around $12\,\text{ms}$ and $18\,\text{ms}$ are caused by the zero-crossing of the arm current. Due to the change in the current direction, the PESBs with the lowest SoC are exchanged for the ones with the highest SoC. This can also be observed in the output voltages and battery module currents in Fig. 6. The exchange of the modules causes a deviation from the fed-forward arm reference voltage from the CCU to the OP4510 impairing the current control. Additionally, the emulator can only set a non-negative output voltage which hinders its ability to enforce a reversal of the current direction.

In the depicted scenario, the current limits for all battery modules are the same as in the simulation which are given in Table I. The current limits for the battery modules are kept within the desired limits most of the time, only in the beginning, when the arm current is increasing, they are exceeded by less than $10\,\%$ of the targeted value.

This could be caused by the dead time between measuring the arm current i_{arm} and the capacitor voltage $v_{\text{C,PEM}}$, calculating the reference output voltage $v_{\text{PESB,ref}}$ of the PESBs and actually setting it. The numerical representation with a limited number of bits of all quantities on the FPGA introduces an additional error. The desired arm voltage is met and the PESBs are selected according to the defined sorting criterion, the SoC. It can be clearly seen in Fig. 6 that the PESB with the lowest SoC, i.e., PESBs 2, 13, 14 and 17, are turned on in the beginning, where the arm reference power p_{arm} is positive and, thus, the battery modules are being charged. However, all of them except for PESB 14 are reducing their output voltage as the arm current increases to fulfill their individual current limitation. Other PESBs are used to still achieve the arm reference voltage. As for the simulation, the used PESBs swap when the current direction changes, as the direction of the arm power also changes.

V. Conclusion

In this work a current-based submodule selection algorithm for a modular multilevel converter based battery energy storage system that allows individual control of the current of each battery module is presented.

Existing submodule selection algorithms do not consider the individual currents of the battery modules and assume an equal load capability of all battery modules within one system. However, to combine different types of battery modules, like high energy, high power or even second-life modules, within one system and to extend their lifetime, the control of the currents of the individual battery modules is required. Thus, the presented, current-based submodule selection algorithm limits the current of the battery modules by limiting the maximum duty cycle of each power electronic storage block based on the measured arm current and the allowed current of the respective battery module. Simulation and experimental results with one arm of an modular multilevel converter based battery energy storage system with an overall energy storage capability of $400\,\mathrm{kWh}$ and a peak power of $100\,\mathrm{kW}$ prove the functionality of the proposed, current-based submodule selection algorithm under test conditions similar to the actual operation of the system.

REFERENCES

[1] Z. Ma, M. Jia, L. Koltermann, A. Blömeke, R. W. De Doncker, W. Li, and D. U. Sauer, "Review on grid-tied modular battery energy storage systems: Configuration classifications, control advances, and performance evaluations," *Journal of Energy Storage*, vol. 74, p. 109272, Dec. 2023.

[2] I. Trintis, S. Munk-Nielsen, and R. Teodorescu, "A new modular multilevel converter with integrated energy storage," in *IECON 2011*. Melbourne, Vic, Australia: IEEE, Nov. 2011.

[3] L. Baruschka and A. Mertens, "Comparison of Cascaded H-Bridge and Modular Multilevel Converters for BESS application," in *2011 IEEE Energy Conversion Congress and Exposition*. Phoenix, AZ, USA: IEEE, Sep. 2011.

[4] M. Schroeder and J. Jaeger, "The idea of a modular multilevel converter with integrated batteries," in *2012 International Conference on Smart Grid Technology, Economics and Policies (SG-TEP)*. Nuremberg, Germany: IEEE, Dec. 2012.

[5] A. Hillers and J. Biela, "Optimal design of the modular multilevel converter for an energy storage system based on split batteries," in *EPE'13*. Lille, France: IEEE, Sep. 2013.

[6] F. Gao, L. Zhang, Q. Zhou, M. Chen, T. Xu, and S. Hu, "State-of-charge balancing control strategy of battery energy storage system based on modular multilevel converter," in *ECCE'14*. Pittsburgh, PA, USA: IEEE, Sep. 2014.

[7] N. Katzenburg, K. Kuhlmann, L. Leister, L. Stefanski, J. Teigelkötter, and M. Hiller, "Design of a Modular Multilevel Converter with 400 kWh of Integrated Batteries," in *2023 22nd International Symposium on Power Electronics (Ee)*. Novi Sad, Serbia: IEEE, Oct. 2023, pp. 1–8.

[8] R. Marquardt, A. Lesnicar, and J. Hildinger, "Modulares Stromrichterkonzept für Netzkupplungsanwendungen bei hohen Spannungen," Jan. 2002.

[9] Z. Ma, F. Gao, X. Gu, N. Li, Q. Wu, X. Wang, and X. Wang, "Multilayer SOH Equalization Scheme for MMC Battery Energy Storage System," *IEEE Transactions on Power Electronics*, vol. 35, no. 12, Dec. 2020.

[10] A. Omar, A. Wood, H. Laird, and P. Gaynor, "Simplified SOC Balancing of an MMC with Embedded Storage in an EV System," in *TENCON 2021 - 2021 IEEE Region 10 Conference (TENCON)*. Auckland, New Zealand: IEEE, Dec. 2021, pp. 929–934.

[11] Z. Ma, F. Yu, X. Zhao, and F. Gao, "The Multidimensional Battery Management Strategy for MMC Battery Energy Storage System," in *2022 IEEE 7th Southern Power Electronics Conference (SPEC)*. Nadi, Fiji: IEEE, Dec. 2022, pp. 1–5.

[12] D. Wang, J. Liu, L. Piegari, S. Song, X. Chen, and D. D. Simone, "A Battery Lifetime Improved Control Strategy of Modular Multilevel Converter for Electric Vehicle Application," in *2019 IEEE 10th International Symposium on Power Electronics for Distributed Generation Systems (PEDG)*. Xi'an: IEEE, Jun. 2019, pp. 594–598.

[13] A. Omar, A. Wood, H. Laird, and P. Gaynor, "Single-Phase Charging of EV Embedded Batteries in an MMC with Submodule Override Capability," *Energies*, vol. 15, no. 6, p. 2276, Mar. 2022.

[14] L. Leister, N. Katzenburg, L. Stefanski, and M. Hiller, "Controlling Battery Lifetime in a Battery Integrated Modular Multilevel Converter," in *2025 10th IEEE Workshop on the Electronic Grid (eGRID)*, Glasgow, 2025.

[15] D&V Electronics Ltd, "DC Emulator - D&V Electronics," https://www.dvelectronics.com/products/emulators/dc-emulator/, Jul. 2025.

[16] OPAL-RT Technologies, "OP4510 Simulator," 2015.

[17] HBK GmbH, "GEN-Serie GEN7tA."

[18] B. Schmitz-Rode, L. Stefanski, R. Schwendemann, S. Decker, S. Mersche, P. Kiehnle, P. Himmelmann, A. Liske, and M. Hiller, "A modular signal processing platform for grid and motor control, HIL and PHIL applications," in *IPEC-Himeji 2022-ECCE Asia*. Himeji, Japan: IEEE, May 2022.

[19] HBK GmbH, "GEN series GN310B (GN311B) - 3 channel power card ± 1500 V DC CAT III and ± 2 A," Aug. 2023.

[20] HBK GmbH, "GEN series GN610B (GN611B) - Isolated 1 kV 2 MS/s (200 kS/s) Input Card," Aug. 2023.

[21] LEM International SA, "Current Transducer LA 55-P," Jul. 2023.

[22] Danisense A/S, "DT50ID - High precision fluxgate AC/DC current transducer for galvanically isolated measurement up to 75 A," Dec. 2023.